Journal of
Ceramic Science
and Technology

J. Ceram. Sci. Technol., **09** [4] 411-418 (2018)
DOI: 10.4416/JCST2018-00035
available online at: http://www.ceramic-science.com
© 2018 Göller Verlag

Low-Temperature Spark Plasma Sintering of a SiC Nanopowder with a Very Thin Al-Based Layer

K. Shimoda*

Research Center for Structural Materials, National Institute for Materials Science,
1-2-1, Sengen, Tsukuba, 305 – 0047 Ibaraki, Japan.

received April 16, 2018; received in revised form May 23, 2018; accepted Juni 14, 2018

Abstract

A SiC nanopowder with an Al-based layer synthesized by means of laser pyrolysis was used to fabricate bulk SiC using spark plasma sintering (SPS) at 1600 – 1800 °C. The surface structure of the novel SiC nanopowder was analyzed by means of field-emission scanning/transmission electron microscopy (FE-SEM/TEM), while the surface chemistry was characterized using X-ray photoelectron spectroscopy (XPS) and energy-dispersive X-ray spectroscopy (EDS). The average particle size was around 45 nm with a very thin (< 5 nm) coating of Al-containing compounds. The effect of the SPS temperature on the density and mechanical and thermal properties of bulk SiC was investigated. Sintered densities above 96 % were obtained at temperatures as low as 1700 °C. Toughened microstructures, which consisted of platelets and relatively small equiaxed SiC grains incorporating crystalline Al_4O_4C, were observed after SPS treatment at 1800 °C. The samples fabricated by means of SPS at 1800 °C had a typical bending strength of 592 MPa, fracture toughness of 5.4 MPam$^{1/2}$, and thermal conductivity of 80 W/mK.

Keywords: SiC, nanopowders, additives, sintering, microstructure

I. Introduction

Silicon carbide (SiC) is one of the most attractive non-oxide ceramic materials for high-temperature structural applications owing to its excellent high-temperature properties, such as a high melting point, high strength, hardness, low thermal expansion, and resistance to oxidation and corrosion. Such favorable properties have facilitated applications in heaters, diesel particulate filters, mechanical seals, and heat exchangers, which all require good mechanical and thermal properties [1–3]. The processing of SiC requires sintering additives to achieve nearly full densification owing to the covalent nature of Si-C bonding and the low self-diffusion coefficient [4]. Sintering SiC ceramics with boron and carbon as sintering additives is becoming a routine method for obtaining dense bulk SiC. However, these materials generally need to be sintered at very high temperatures (> 2000 °C) and exhibit a coarse microstructure and poor mechanical properties; for example, a bending strength of ~ 500 MPa and fracture toughness ~ 3 MPa m$^{1/2}$ owing to reduced flaw tolerance [5–7]. Recently, additive-free SiC has been developed. However, very high temperatures under extremely high pressures during sintering are required for the densification of additive-free SiC [8–10]. Nadeau reported that the nearly full densification of SiC without additives can be achieved under 2500 °C and applied pressure of 5 GPa by means of hot pressing [8]. With spark plasma sintering (SPS), which is a very powerful method for preparing ceramic materials that are difficult to sinter in conventional hot-pressing, bulk SiC using pure SiC powder without additives has been obtained in relatively moderate sintering conditions [10–12]. Maitre *et al.* reported that a relatively high sintering temperature of 1950 °C and applied pressure of 100 MPa with SPS was required to obtain dense bulk SiC using pure SiC powder [11]. To reduce the sintering temperature and increase the low fracture toughness of bulk SiC, liquid phase sintering (LPS) of SiC nanopowder (with a particle size < 100 nm) has been a focus over the last decades as this material has a high sintering rate owing to its high surface area and short diffusion distance of the chemical species [13–16]. The most important factors that control LPS of SiC are: (1) the quality of the SiC nanopowder starting material; (2) conditions such as the temperature, atmosphere, applied stress, and dwell time during sintering; (3) the composition and amount of liquid phase sintering additive; and (4) the method used to mix the SiC nanopowder and sintering additives. However, SiC nanopowder is usually covered with impurity phases, such as additional carbon, silica (SiO_2), and siliconoxycarbide (SiO_xC_y), which have various effects on the sintering process of SiC, including selection of the composition and amount of sintering additives, the dispersion of the SiC nanopowder and sintering additives during mixing, and the sintering conditions (temperature and dwell time) [17,18]. Generally, a sintering temperature of ~ 2100 °C was used in N_2 and ~ 1900 °C in Ar for a dwell time of ~2 h, with or without applied pressure [19].

Various sintering additives have been investigated for the formation of the liquid phase used to improve sinterability and promote higher fracture toughness. Examples

* Corresponding author: SHIMODA.Kazuya@nims.go.jp

of well-known sintering additives are mixtures of Al_2O_3 or AlN with rare-earth oxides (Y_2O_3, La_2O_3, Sm_2O_3, Tb_2O_3) [20–22]. It is quite important to control the morphology of the sintering additives during sintering as the intergranular remnants of excess additives, which generally include a partly amorphous phase, strongly affect the mechanical and thermal properties of SiC sintered by means of LPS. This amorphous phase, which can soften and vaporize at elevated temperatures, causes sever degradation of the high-temperature strength and creep resistance as well as of the oxidation resistance [23]. In addition, for high-temperature applications, homogeneous dispersion of the sintering additives in sintered SiC is required as the intergranular remnants from excess additives can act as nucleation points for fracture and creep; however, such ideal mixing has been difficult to achieve to date.

In this study, we explored a new method for enhancing sinterability of SiC at lower temperatures below 1800 °C; we used a novel SiC nanopowder, designed to enhance sinterability, onto which a layer of Al-containing additive is coated with a controlled thickness less than 10 nm. This novel starting material was processed using SPS. This method is thought to avoid problematic mixing processes, such as magnetic stirring or ball milling, and achieve homogeneous distribution of the additives in the sintered bulk SiC. The aim of this study was to characterize this novel SiC nanopowder based on microstructural observations and surface chemical analyses, and investigate whether this nanopowder could be used in an SPS process to produce dense SiC at temperatures lower than 1800 °C. In addition, the thermal and mechanical properties of SPS-formed SiC are discussed here, based on the evolution of the microstructure compared to that of conventional SPS SiC using a pure SiC nanopowder with and without sintering additives

II. Experimental Procedure

(1) Material preparation

A novel SiC nanopowder was used in this study as a starting material and was manufactured by Nanomakers (France). A layer of Al-containing sintering additive was coated onto the pure SiC nanopowder (Nanomakers, France, NM SiC99, mean diameter of 35 nm, 99.999 % purity) with a controlled thickness below 10 nm using the laser pyrolysis method and with heating at around 1000 °C. Trimethylaluminum ($Al(CH_3)_3$), an organometal of aluminum, was employed as a source for the Al-containing layer. The crystalline phase of the novel SiC nanopowder was identified by means of X-ray diffraction (XRD; RINT-2500, Rigaku, Japan) using CuKα radiation. The SiC nanopowder was analyzed using both field-emission scanning electron microscopy (FE-SEM; Ultra 55, ZEISS, Germany) and field-emission transmission electron microscopy (FE-TEM; JEM-2200FS, JEOL, Japan) to characterize the morphological features and particle size distribution. The chemical composition was analyzed using energy-dispersive X-ray spectroscopy (EDS) system integrated with the FE-TEM. The surface chemistry of the SiC nanopowder was characterized using X-ray photoelectron spectroscopy (XPS; PHI Quantum 2000) using AlKα (1486.6 eV) radiation. The SiC nanopowder was sintered using an SPS system (SPS-5104A, Syntex Inc., Japan) at various temperatures between 1600 and 1800 °C under a pressure of 50 MPa in Ar, with a heating rate of 100 K/min. After a dwell time of 10 min, the samples were cooled in the furnace to the ambient temperature of 25 °C at the natural cooling rate of the furnace.

(2) Evaluation of the sintered SiC

The density values of the SPS-formed SiC were determined based on the Archimedes principle using pure water as the immersion medium. The microstructures of the sintered SiC were characterized by means of FE-SEM, FE-TEM, scanning TEM, EDS, while the crystal structure was analyzed using XRD. Bending test specimens for characterizing the mechanical properties were cut from the bulk SPS SiC samples with dimensions of 3 × 1.5 × 22 mm^3 (width, thickness, and length, respectively) and then polished on four sides to a mirror surface with a 1- – 3-μm diamond slurry. Three-point bending tests were undertaken on five specimens for each sample type with a crosshead speed of 0.1 mm/min and an outer support span of 18 mm at the ambient temperature of 25 °C, using an INSTRON 5581 test machine. The bending stress (σ) and modulus of the elasticity in bending (E) were calculated using Eqs. (1) and (2), respectively.

$$\sigma = 3PL/2\,wt^2 \quad (1)$$

$$E = 0.25L^3n/wt^3 \quad (2)$$

where P is the maximum load at a given point, L is the outer support span, w is the specimen width, t is the specimen thickness, and n is the slope of the tangent to the initial linear portion of the load-deflection curve. The fracture surfaces were examined with FE-SEM. In addition, Vickers hardness (H_v) and fracture toughness (K_{IC}) tests were performed using the test number of five. The H_v values were measured at an applied load of 19.6 N for 15 s. The indentation fracture method was used to obtain the K_{IC} values.

For thermal conductivity measurements, the dimensions of the sintered SiC sample were about 10 mm in diameter and about 2 mm in thickness. The thermal diffusivity and heat capacity at the face perpendicular to the direction of uniaxial pressing during SPS were measured using a laser flash technique at the ambient temperature of 25 °C in air using a TC7000 test machine (ULVAC-RIKO, Inc. Japan). The measured sample number was three. The thermal diffusivity (a) was determined using the $t_{1/2}$ method from the following equation [24]:

$$\alpha = 1.38L^2/\pi^2 t_{1/2} \quad (3)$$

where $t_{1/2}$ is the time required to reach half of the total temperature increase on the near specimen and L is the thickness of specimen. The thermal conductivity (K) in the direction through the thickness was calculated using:

$$K = \alpha\varrho C_v \quad (4)$$

where a is the thermal diffusivity, ϱ is the density, and C_v is the specific heat. The obtained mechanical and thermal behavior were compared with that of a pure SiC nanopowder reference sample (Nanomakers, France, NM SiC99, mean diameter of 35 nm, 99.999 % purity) with and without a sintering additive (6 wt% Al_2O_3 (Kojundo Chemi-

cal Laboratory Co. LTD., Japan, mean diameter of 0.3 µm, 99.99 % purity)-4 wt% Y_2O_3 (Kojundo Chemical Laboratory Co. LTD., Japan, mean diameter of 0.4 µm, 99.99 % purity).

III. Results

(1) Novel SiC nanopowder properties

(a) *Crystal structure*

Fig. 1 shows the diffraction pattern of the novel SiC nanopowder. The positions of the diffraction lines matched well with those from the powder diffraction database (JSPDF) as (h k l) = (1 1 1), (2 0 0), (2 2 0), (3 1 1), and (2 2 2), corresponding to 3C (β)-SiC with stacking faults. Other diffraction peaks were assigned to aluminum hydroxide ($Al(OH)_3$).

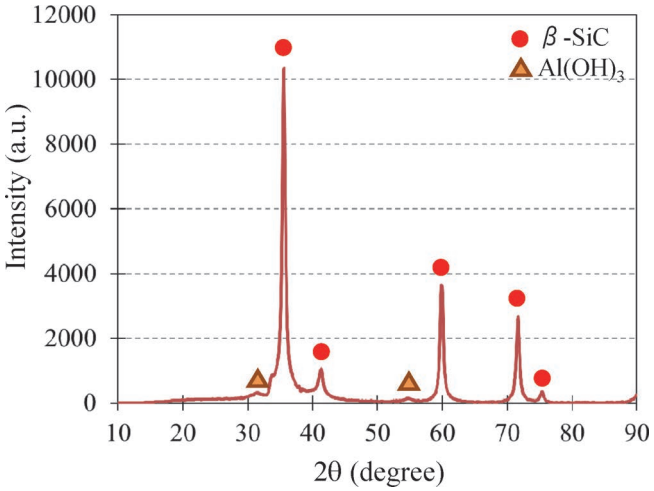

Fig. 1: XRD pattern of the novel SiC nanopowder.

(b) *Morphology and particle size distribution*

Fig. 2(a) shows FE-SEM images of the novel SiC nanopowder. The average particle size distribution obtained from several FE-SEM images is shown in Fig. 2(b). The average particle size of the novel SiC nanopowder was around 45 nm with a sharp distribution peak, which was well-controlled to < 100 nm. Fig. 3(a) – (c) show TEM images of the novel SiC nanopowder, high-resolution TEM images of the nanopowder surface, and EDS elemental analysis of selected points, respectively. The nanoparticles were almost spherical, where several neighboring grains were probably interconnected by covalent bonds. High-resolution TEM images of the novel SiC nanopowder showed a very thin layer (~ 5 nm) on its surface, where Si, C, Al, and O were detected with EDS point analysis. In conclusion, the morphology of the novel SiC nanopowder was almost spherical with a core-shell structure, as shown in Fig. 4.

(c) *Surface chemistry*

Detailed chemical characterization of the surface layer on the novel SiC nanopowder was performed using XPS, which is a useful technique for identifying surface impurities on SiC powers by analyzing the chemical bonds [17,18]. The present authors previously reported that commercially available SiC nanopowders are generally covered with surface impurities such as silica (SiO_2), siliconoxycarbide (SiO_xC_y), and/or free carbon [17]. In this work, photoelectrons were generated within the X-ray penetration depth (typically microns), but only those within the top three photoelectron escape depths were detected; the escape depth was of the order of 1.5 – 3.5 nm, corresponding to an analysis depth of 5 – 10 nm. According to the overall spectra for the novel SiC nanopowder in the binding energy region of 0 – 700 eV, O-based bonds (O1s peak), C-based bonds (C1s peak), Al-based bonds (Al2s and Al2p peaks), and Si-based bond (Si2s and Si2p peaks) were detected, as shown in Fig. 5. Fig. 6 shows the results of XPS scans on the novel SiC nanopowder over narrow ranges, around the peaks of O_{1s} (E_b = 542 – 525 eV), C_{1s} (E_b = 292 – 278 eV), Al2p (E_b = 85 – 65 eV), and Si2p (E_b = 107 – 97 eV). The atomic fractions based on O1s, C1s, Al2p, and Si2p peaks measured for the surface of the novel SiC nanopowder are shown in Table 2. The values were normalized to 100 % using the elements detected, where the detection limits were approximately 0.05 to 1.0 at%. The novel SiC nanopowder was composed primarily of C, O, and Si with somewhat lower levels of Al (see Table 1). Aluminum was found as a combination of Al-metal (Al^0), corresponding to the peak at 71.8 eV,

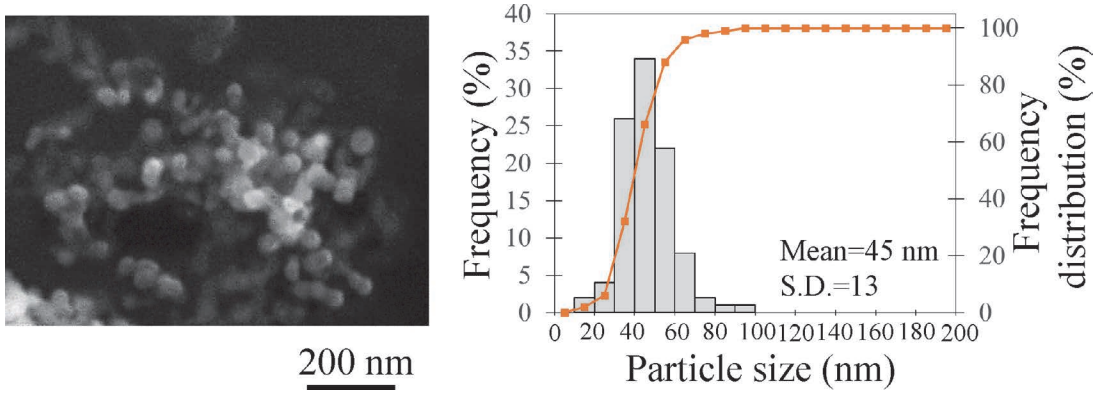

Fig. 2: FE-SEM images and particle size distribution of the novel SiC nanopowder.

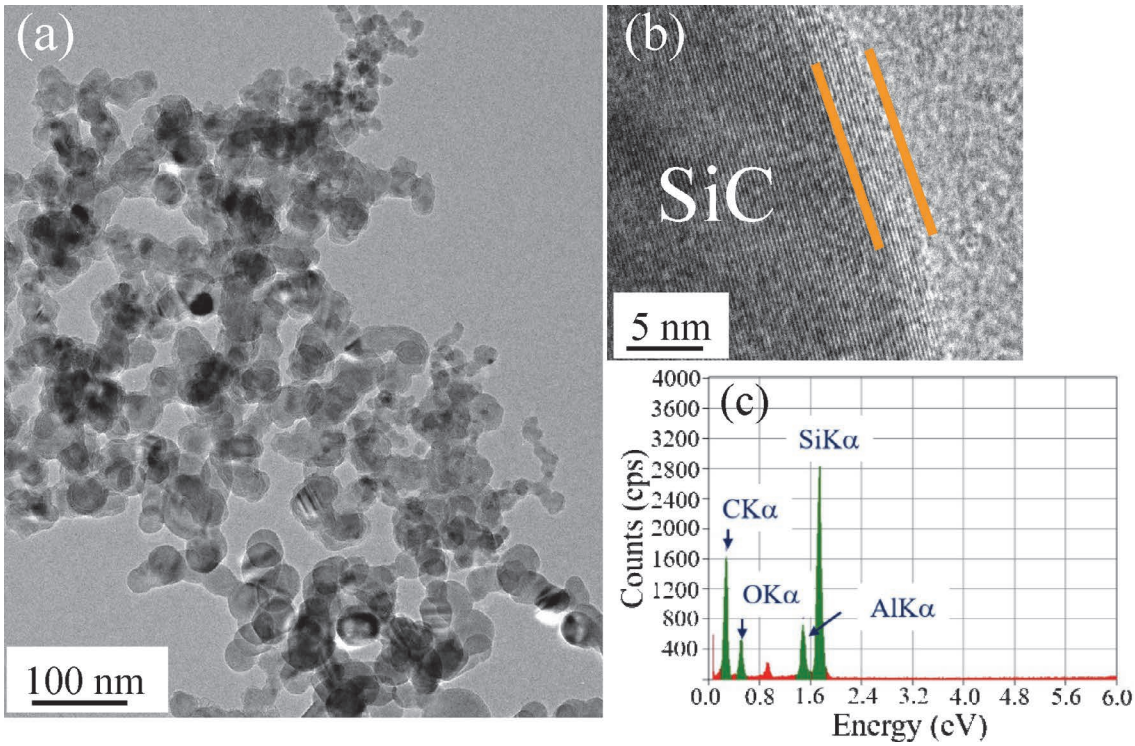

Fig. 3: (a) TEM image of the novel SiC nanopowder, (b) high-resolution TEM image near the novel SiC nanopowder surface, and (c) EDS elemental analysis.

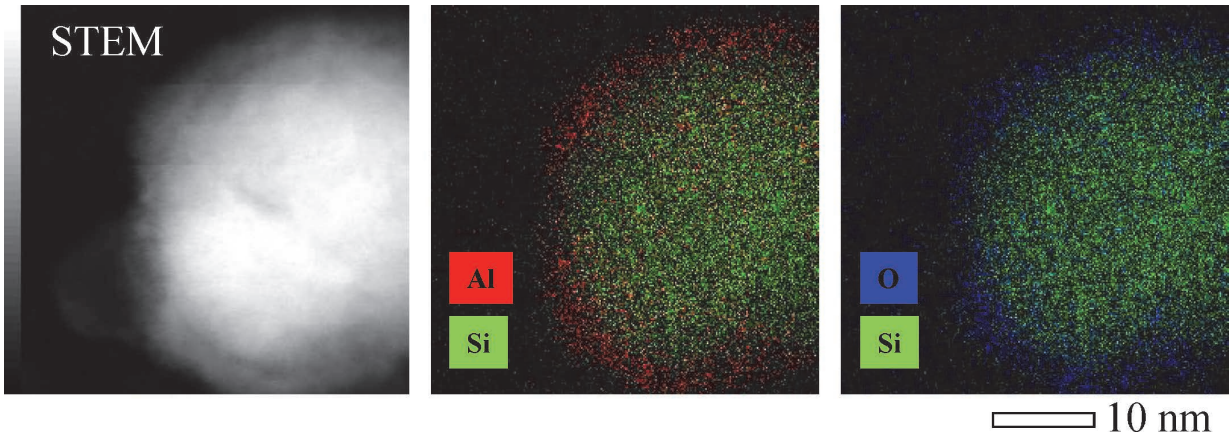

Fig. 4: EDS mapping of the SiC nanoparticle.

Table 1: Atomic concentrations measured with XPS from the surface of the novel SiC nanopowder.

	C (at%)	O (at%)	Al (at%)	Si (at%)
Novel SiC nanopowder	40 ± 0.2	24 ± 0.9	12 ± 0.1	24 ± 0.9

Values normalized to 100 % of the elements detected.

and Al-hydroxide ($Al(OH)_3$), attributed to the peak at 74.5 eV [25]. The binding energy and O concentration suggested that the higher binding energy component was due to $Al(OH)_3$, although the presence of Al_2O_3 cannot be ruled out. Silicon was found exclusively as Si-C. Carbon was found primarily as the carbide (i.e. SiC) with lower levels of hydrocarbon and carbon oxygen functionalities. Oxygen was found as $Al(OH)_3$ (532.8 eV), Al-oxides (531.3 eV), and organic species [17,25].

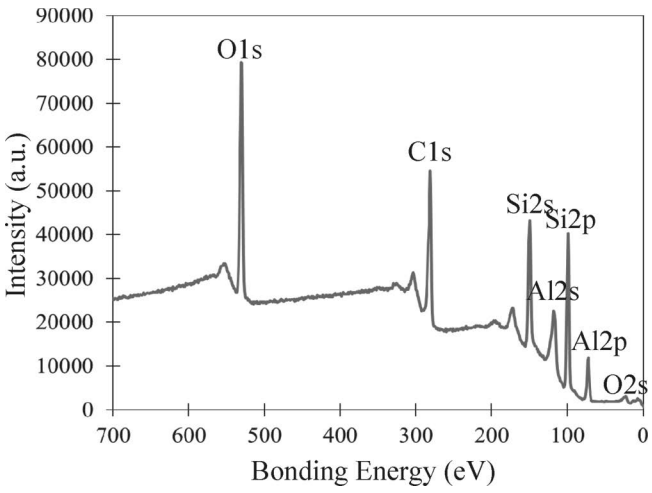

Fig. 5: Overall XPS spectra of the novel SiC nanopowder.

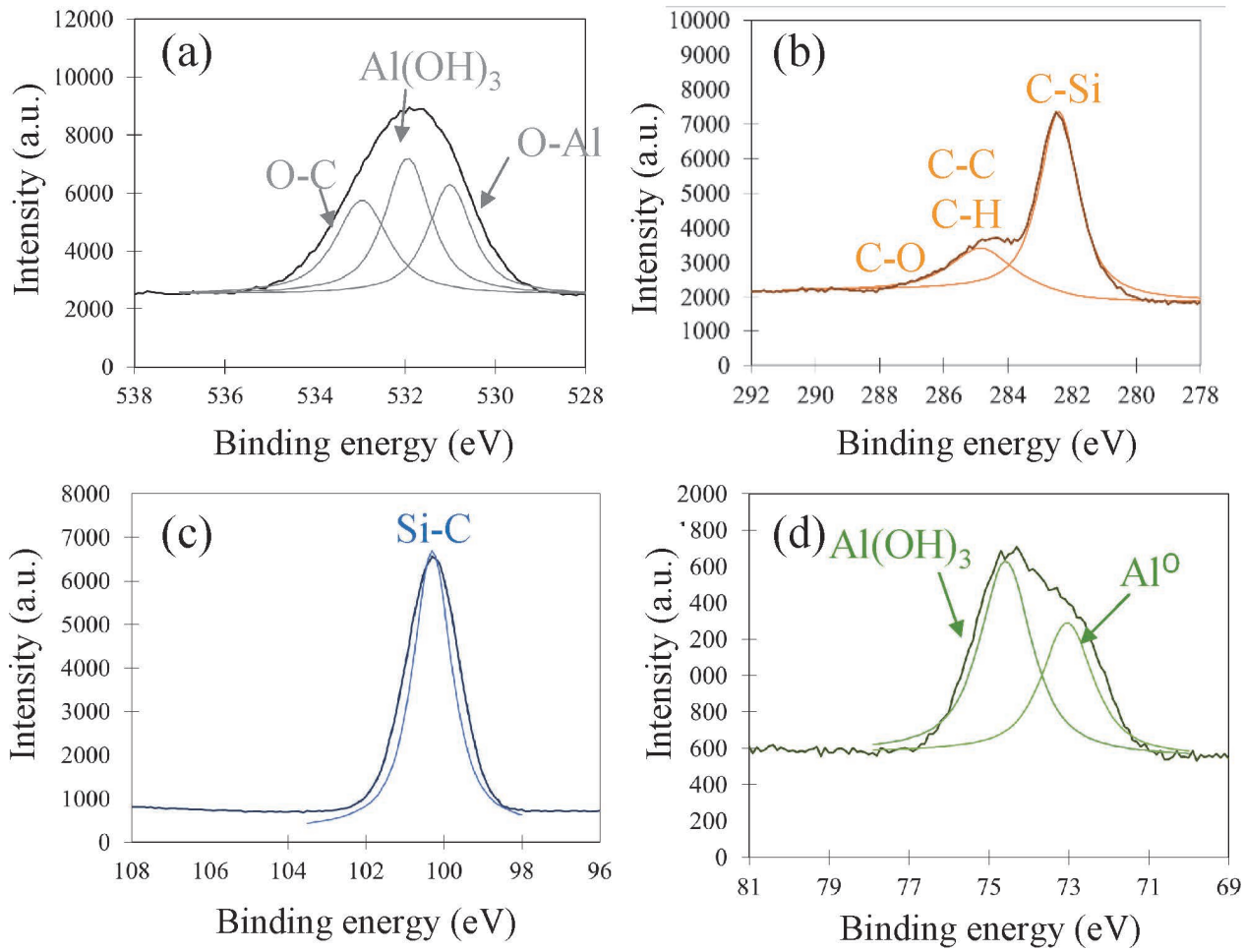

Fig. 6: XPS spectra of the novel SiC nanopowder. (a) O1s, (b) C1s, (c) Si2>p, and (d) Al2p peaks.

(2) Properties of bulk sintered SiC

Table 2 summarizes the results of the densification, thermal, and mechanical tests of the bulk SiC sintered by SPS at 1600 – 1800 °C; samples prepared using the novel SiC nanopowder with a very thin Al-based coating or pure SiC nanopowder with or without sintering additives were compared. With increasing sintering temperature, the density increased, and all thermal and mechanical properties were enhanced. SPS-treated samples with densities above 96 % were achieved at a temperature as low as 1700 °C, the highest density being obtained at 1800 °C with typical bending strength of 592 ± 55 MPa, fracture toughness of 5.4 ± 0.18 MPam$^{1/2}$, and thermal conductivity of 80 ± 0.41 W/mK at the ambient temperature of 25 °C, for the novel SiC nanopowder. These values were significantly higher than those of the conventional SiC treated by means of SPS at 1800 °C using the pure SiC nanopowder with or without sintering additives.

Fig. 7 shows the diffraction pattern of SiC sintered at 1600 – 1800 °C, which clearly showed the existence of the α-SiC polytype (indexed as JSPDF:89 – 1396) and crystalline Al_4O_4C (indexed as JSPDF:48 – 1583). The sharpest peaks for the α-SiC and Al_4O_4C phases were detected in the sample sintered at 1800 °C. Fig. 8 shows back-scattered electron images of SPS-sintered SiC at 1600 – 1800 °C taken from a polished surface. At 1600 °C, many pores were observed, resulting in a lower density (as shown in Table 2). At 1700 and 1800 °C, many dark areas were observed, which were identified as the Al_4O_4C phase with EDS analysis. Fig. 9 shows secondary electron images (SEIs) of the fracture surfaces of SiC sintered at 1600 – 1800 °C. With increasing temperature, densified and toughened microstructures and SiC grain growth were observed. In particular, significant grain growth of Al_4O_4C and SiC by ~ 300 nm at 1800 °C was observed.

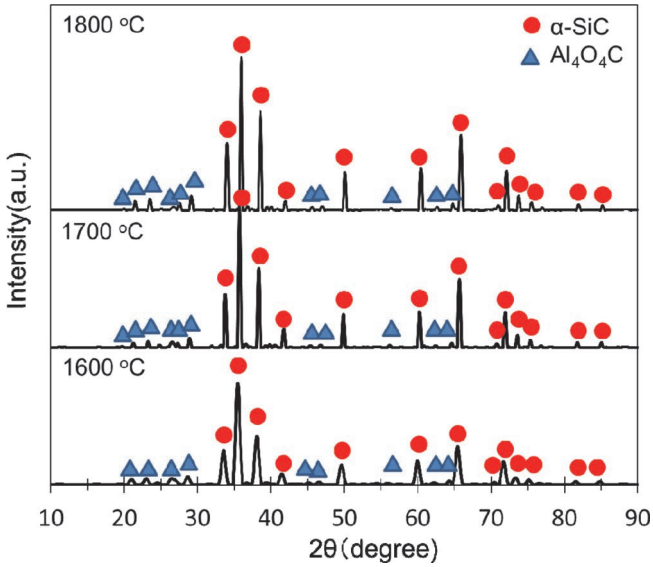

Fig. 7: XRD patterns for SiC formed by SPS at 1600 – 1800 °C.

Table 2: Summary of the properties of bulk SiC produced by means of SPS.

Powder + additives	Sintering Temperature (°C)	Bulk density (g/cm^3)	Relative density (%)	Bending strength (MPa)	Vickers hardness (GPa)	Fracture toughness (MPa · m$^{1/2}$)	Thermal conductivity (W/mK)
100 wt% novel SiC nanopowder	1600	2.81	93	416±33	22.6±0.94	4.6±0.19	41±1.2
100 wt% novel SiC nanopowder	1700	3.00	96	505±45	26.5±1.7	5.0±0.20	62±0.90
100 wt% novel SiC nanopowder	1800	3.08	97	592±55	27.5±1.4	5.4±0.18	80±0.41
100 wt% pure SiC nanopowder	1800	2.18	67	118±13	N/D	N/D	N/D
90 wt% pure SiC nanopowder + 6 wt% Al_2O_3-4 wt% Y_2O_3	1800	3.05	95	522±43	25.2±1.8	4.6±0.31	46±1.6

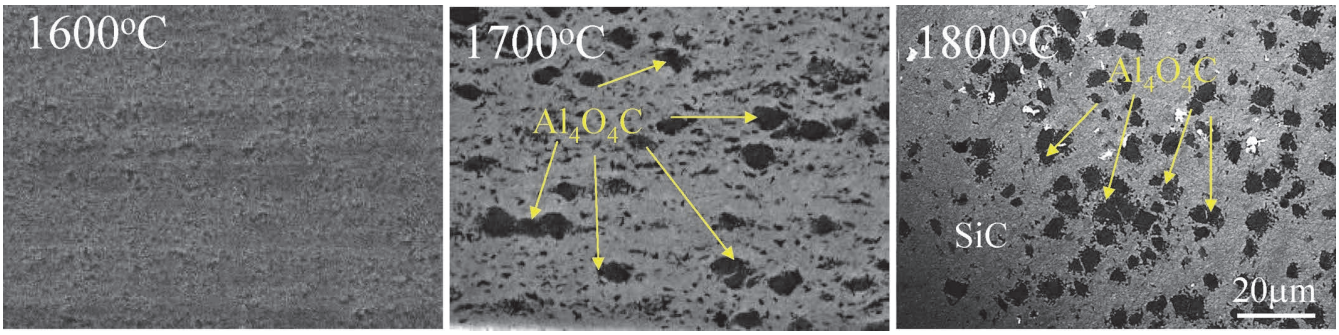

Fig. 8: Back-scattered electron images of SPS-sintered SiC at 1600 – 1800 °C taken from a polished surface.

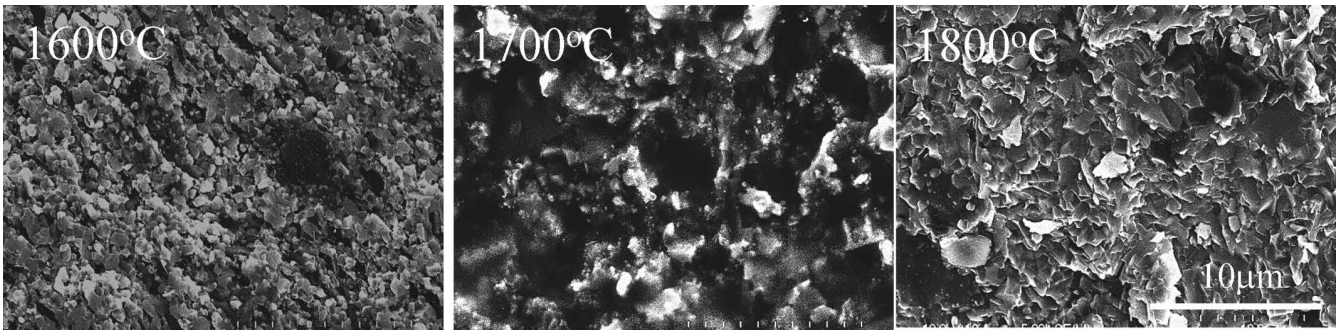

Fig. 9: Secondary electron images of the fracture surfaces of SPS-sintered SiC at 1600 – 1800 °C.

IV. Discussion

Al-based additives in SiC ceramics are suitable for a wide range of applications. Owing to He gas production under neutron irradiation, boron cannot be used as sintering additives for nuclear applications, where SiC is promising as nuclear fuel coating and core components for future reactors [26]. The properties of the sintered SiC are significantly affected by the type and amount of additive and the processing conditions used for consolidation. The homogeneous dispersion of additives in sintered SiC is important for high-temperature applications as intergranular residues owing to the fact that excess additives can act as nucleation sites for fracture and creep; however, ideal mixing has been challenging to date [18].

In this study, we used a novel SiC nanopowder with a very thin coating of a sintering additive as a starting material to enhance compositional homogeneity and avoid complicated mixing processes. High-resolution TEM images confirmed that the SiC nanoparticles were covered with a very thin (< 5 nm) layer, which contained Al and O (from EDS point analysis and mapping. In addition, the use of the novel SiC nanopowder reduced the sintering temperature, which is advantageous for producing these materials, e.g. energy savings and fewer undesirable side-reactions.

In this study, SPS was employed to densify the SiC samples at temperatures below 1800 °C. Compared to conventional hot-pressing, SPS can sinter ceramics at lower temperatures in shorter times. Although SPS is similar to hot-pressing, instead of indirect heating, both the die and the powder compact are heated by an applied electrical current. For the novel SiC nanopowder, SPS sintering at 1600 °C resulted in a compact with a relative density of 93 %, while a temperature above 1700 °C resulted in rel-

ative densities of 96 % or more. On the other hand, for pure SiC nanopowder with no addition of sintering additives, even an SPS temperature of 1800 °C yielded relative densities less than 70 %, which resulted in the low bending strengths. This might be due to the poor sintering conditions (temperature and applied pressure) for densification [8–10]. For pure SiC nanopowder with Al_2O_3-Y_2O_3 additives, SPS at 1800 °C resulted in samples with a relative density of 94 %. Tamari *et al.* reported that the density of SiC containing Al_2O_3-Y_2O_3 processed using SPS, even under a relatively low applied pressure of 30 MPa for a short dwell time of 5 min, was over 90 % at 1800 °C; this is above the eutectic phase point of $Al_2O_3 - Y_2O_3$ (T_{EU} = 1760 °C) [27,28]. Here, the mechanical properties of the samples produced by means of SPS using the novel SiC nanopowder improved with increasing sintering temperature. The typical properties of a sample processed with SPS at 1800 °C were a strength of 592 ± 55 MPa, Vickers hardness of 27.5 ± 1.4 GPa, and fracture toughness of 5.4 ± 0.18 MPa $m^{1/2}$; these values were significantly higher than those of the SPS SiC prepared using the pure SiC nanopowder, even with sintering additives. Here, although the pure SiC nanopowder showed the β-SiC phase, XRD analysis showed peaks for α-SiC after SPS (Fig. 7).

β-SiC is not stable at high temperatures and it is well known that a transformation of β-to α-SiC occurs in a temperature range of 1600 – 1900 °C [29]. This transformation depends on several parameters during sintering, such as sintering temperature, additives, and atmosphere [29–32]. Moreover, the layer of Al-containing additives may promote this β-to α-SiC transformation. Kim *et al.* and Lee *et al.* reported that α-SiC powder as a starting material often produces an equiaxed microstructure, while a platelet microstructure is often observed for β-SiC [33,34]. When β-SiC powder is employed as a starting material, this transformation can contribute to enhancing the fracture toughness owing to a crack-bridging mechanism.

In addition, the thermal conductivity after SPS of the novel SiC nanopowder improved with increasing temperature. At 1800 °C, the thermal conductivity was approximately 80 ± 0.41 W/mK, which was higher than that of the SPS sample using pure SiC nanopowder with the sintering additives. The intrinsic thermal conductivity of SiC is considered to be 490 W/mK [35]. Generally, polycrystalline SiC shows a thermal conductivity of 30 – 270 W/mK, which is much lower than the intrinsic value. In particular, LPS SiC incorporating Al-containing additives showed a relatively low conductivity of 30 – 80 W/mK [36]. Here, SPS of the pure SiC nanopowder with sintering additives (6 wt% Al_2O_3-4 wt% Y_2O_3) exhibited a thermal conductivity of 46 ± 1.6 W/mK. However, the SPS sample using the novel SiC nanopowder exhibited a relatively high thermal conductivity of 80 ± 0.41 W/mK. This was mainly because the β → α phase transformation of SiC occurred. The effect of this transformation on the thermal conductivity has not been systematically studied. Sakai *et al.* reported that SiC with Al_2O_3 showed a gradual decrease in thermal conductivity with increasing amount of the 4H polytype, which was produced from the β-SiC powder as a starting material [37]. Grain growth appeared to be beneficial for enhancing the thermal conductivity of SiC; here, significant grain growth was observed with increasing temperature; at 1800 °C a growth of ~ 300 nm was observed (Fig. 8).

The chemistry of the sintering additive also dramatically affects the thermal conductivity of polycrystalline SiC. Here, crystalline Al_4O_4C was observed as a secondary phase with XRD analysis. During SPS, the novel SiC nanopowder with a very thin Al-based coating formed Al_2O_3 on the dehydration reaction of $Al(OH)_3$ at around 180 °C, giving off water vapor:

$$Al(OH)_3(s) \rightarrow Al_2O_3(s) + 3H_2O(g) \quad (5)$$

The formed Al_2O_3 would generate Al_2O gas according to Eq. (6):

$$Al_2O_3(s) + 4Al(l) = 3Al_2O(g) \quad (6)$$

Reactions between the metallic aluminum and Al_2O_3 or Al_2O gas and Al_2O_3 form Al_4O_4C according to Eq. (7) and (8), respectively:

$$4Al_2O_3(s) + 4Al(l) + 3C(s) = 3Al_4O_4C(s) \quad (7)$$

$$Al_2O(g) + Al_2O_3(s) + C(s) = Al_4O_4C(s) \quad (8)$$

Carbon might come from CO gas because a carbon die was used under Ar atmosphere in this study. With increasing SPS temperature, the volumetric ratio of Al_4O_4C increased, with significant grain growth of Al_4O_4C and SiC. At 1800 °C, the grain size of Al_4O_4C was almost the same as that of SiC. The relatively high thermal conductivity and fracture toughness could be attributed to this crystalline Al_4O_4C. Hence, Al_4O_4C is a promising candidate as a reinforcement phase in SiC for high-temperature applications owing to its low density and high stability against heat and oxidation [38,39].

V. Conclusions

To avoid mixing processes that can be problematic in respect of inhomogeneous phases, a new method for achieving nearly fully dense SiC at low temperatures below 1800 °C was demonstrated using a novel SiC nanopowder and SPS. The morphology of the novel SiC nanopowder was almost spherical and had a core-shell structure. The average particle size was around 45 nm with a < 5 nm coating of Al-containing additives that reinforced the SiC. Relative densities above 96 % were obtained after SPS at temperatures as low as 1700 °C. The pure SiC nanopowder without sintering additives could not reach full densification under SPS conditions at 1800 °C. Even in the case of the pure SiC nanopowder with sintering additives, significant improvement in the fracture toughness and thermal conductivity did not occur after SPS at 1800 °C. Toughened microstructures, which consisted of platelets and relatively small equiaxed SiC grains with the Al_4O_4C crystalline phase, were produced after SPS at 1800 °C. Typical bending strength, fracture toughness, and thermal conductivity values of samples prepared by means of SPS at 1800 °C were 592 ± 55 MPa, 5.4 ± 0.18 MPa $m^{1/2}$, and 80 ± 0.41 W/mK, respectively. This study has demonstrated a facile method for producing SiC material with enhanced sinterability and superior thermal and mechanical properties compared to standard processes.

Acknowledgment

The author would like to thank Dr Nishimura at National Institute for Materials Science (NIMS) for his help with the SPS operation.

References

1 Nakamura, K., Maeda, K.: Silicon Carbide Ceramics, Vol. 2, Elsevier, Barking, 1991.

2 Dapkunas, S.J.: Ceramic heat exchangers, *Am. Ceram. Soc. Bull*., **67**, 388 – 391, (1988).

3 Willinder, M., Friesel, M., Qamar-ul, W., Straumal, B.: Silicon carbide and diamond for high temperature device applications, *J. Mater. Sci*., **17**, 1 – 25, (2006).

4 Haris, G.L.: Properties of Silicon Carbide. G.L. Haris (Ed.), INSPEC, London, 1995.

5 Prochazka, S., Scanlan, R.M.: Effect of boron and carbon on sintering of SiC, *J. Am. Ceram. Soc*., **58,** 72, (1975).

6 Zhou, Y., Tanaka, H., Otani, S., Bando, Y.: Low-temperature pressureless sintering of α-SiC with Al_4C_3-B_4C-C additions, *J. Am. Ceram. Soc*., **82**, 1959 – 1964, (1999).

7 Ghosh, A., Jenkins, M.G., White, K.W., Kobayashi, A.S., Brad, R.C.: Elevated-temperature fracture resistance of a sintered alpha-silicon carbide, *J. Am. Ceram. Soc*., **72**, 242 – 247, (1989).

8 Nadeau, J.S.: Very high pressure hot pressing of silicon carbide, *J. Am. Ceram. Soc. Bull*., **52** 170 – 174, (1973).

9 Xie, M.L., Luo, D.L., Xian, X.B., Leng, B.Y., Chen, C., Lu, W.Y.: Densification of nano-SiC by ultra-high-pressure effect of time, temperature and pressure, *Fusion Eng. Des*., **85**, 964 – 968, (2010).

10 Yamamoto, T., Kitaura, H., Kodera, Y., Ishii, T., Ohyanagi, M., Munir, Z.A., Consolidation of nanostructure β-SiC by spark plasma sintering, *J. Am. Ceram. Soc*., **87**, 1436 – 1441, (2004).

11 Maitre, A., Vande Put, A., Laval, J.P., Valette, S., Trolliard, G.: Role of boron on the spark plasma sintering of an α-SiC powder, *J. Eur. Ceram. Soc*., **28**, 1881 – 1890, (2008).

12 Munir, Z.A., Anselmi-Tamburini, U., Ohyanagi, M.: The effect of electric field and pressure on the synthesis and consolidation of materials: A review of the spark plasma sintering method, *J. Mater. Sci*., **41**, 763 – 777, (2006).

13 Kijima, K., Noguchi, H., Konishi, M.: Sintering of ultrafine SiC powders prepared by plasma CVD, *J. Mater. Sci*., **24**, 2929 – 2933, (1989).

14 Kim, Y.W., Lee, Y.I., Mitomo, M.: Sinterability of nano-sized silicon carbide powders, *J. Ceram. Soc. Jpn*., **114**, 681 – 685, (2006).

15 Shimoda, K., Park, J.S., Hinoki, T., Kohyama, A.: Densification mechanism and microstructural evolutions of SiC matrix in NITE process, *Ceram. Eng. Sci. Proc*., **27**, 19 – 27, (2006).

16 Malinge, A., Coupe, A., Petitcorps, Y.L., Pailler, R.: Pressureless sintering of beta silicon carbide nanoparticles, *J. Eur. Ceram. Soc*., **32**, 4393 – 4400, (2012).

17 Shimoda, K., Park, J.S., Hinoki, T., Kohyama, A.: Influence of surface structure of SiC nano-sized powder analyzed by X-ray photoelectron spectroscopy on basic powder characteristics, *Appl. Surf. Sci*., **253**, 9450 – 9456, (2007).

18 Shimoda, K., Koyanagi, T.: Surface properties and dispersion behaviors of SiC nanopowders, *Colloid. Surf. A*., **463**, 93 – 100, (2014).

19 Raju, K., Yoon, D.H.: Sintering additives for SiC based on the reactivity: A review, *J. Ceram. Int*., **42**, 17947 – 17962, (2016).

20 Omori, M., Takei, H.: Pressureless sintering of SiC, *J. Am. Ceram. Soc*., **65**, C92 – C96, (1982).

21 Noviyanto, A., Yoon, D.H.: Rare-earth oxide additives for the sintering of silicon carbide, *Diam. Relat. Mater*., **38**, 124 – 130, (2013).

22 Taguchi, S.P., Motta, F.V., Balestra, R.M., Riberio, S.: Wetting behavior of SiC ceramics. Part II-Y_2O_3/Al_2O_3 and Sm_2O_3/Al_2O_3, *Mater. Lett*., **58**, 2810 – 2814, (2004).

23 Shimoda, K., Kondo, S., Hinoki, T., Kohyama, A.: Thermal stress relaxation creep and microstructural evolutions of nanostructured SiC ceramics by liquid phase sintering, *J. Eur. Ceram. Soc*., **30**, 2643 – 2652, (2010).

24 Parker, W.J., Jenkins, R.J., Butler, C.P., Abbott, G.L.: Flash method of determining thermal diffusivity, heat capacity, and thermal conductivity, *J. Appl. Phys*., **32**, 1679 – 1684, (1961).

25 Strohmeier, B.R.: An ESCA method for determining the oxide thickness on aluminum alloys, *Surf. Interface. Anal*., **15**, 51 – 56, (1990).

26 Lee, C.W., Pineau, F.J., Corelli, J.C.: Thermal properties of neutron-irradiated SiC; effects of boron doping, *J. Nucl. Mater*., **108**, 678 – 684, (1982).

27 Tamari, N., Tanaka, T., Tanaka, K., Kondoh, I., Kawahara, M., Tokita, M.: Effect of spark plasma sintering on densification and mechanical properties of silicon carbide, *J. Ceram. Soc. Jpn*., **103**, 740 – 742, (1995).

28 Levin, E.M., Robbins, C.R., McMurdie, H.E.: Phase diagrams for ceramists, The American Ceramic Society, Inc., 1969, pp. 165.

29 Xu, H., Bahtia, T., Deshpande, S.A., Padture, N.P., Ortiz, A.L., Cumbrera, F.L.: Microstructural evolution in liquid-phase-sintered SiC: part I, effect of starting powder, *J. Am. Ceram. Soc*., **84**, 1578 – 584, (2001)

30 Ragaru, C., Lancin, M., Marhic, C.: β→α phase transformation in SiC: link between polytypism, dihedral angle and nucleation mechanism of α twins, *J. Eur. Ceram. Soc*., **19**, 2701 – 2709, (1999).

31 Zawrah, M.F., Shaw, L.: Liquid-phase sintering of SiC in presence of CaO, *Ceram. Int*., **30**, 721 – 725, (2004).

32 Gomez, E., Echeberria, J., Iturriza, I., Castro, F.: Liquid phase sintering of SiC with additions of Y_2O_3, Al_2O_3 and SiO_2, *J. Eur. Ceram. Soc*., **24**, 2895 – 2903, (2004).

33 Kim, Y.W., Mitomo, M., Emoto, H., Lee, J.G.: Effect of initial α-phase on microstructure and mechanical properties of sintered silicon carbide, *J. Am. Ceram. Soc*., **81**, 3136 – 3140, (1998).

34 Lee, J.K., Park, J.G., Lee, E.G., Seo, D.S., Hwang, Y.: Effect of starting phase on microstructure and fracture toughness of hot-pressed silicon carbide, *Mater. Lett*., **57**, 203 – 208, (2002).

35 Slack, G.A.: Thermal conductivity of pure and impure silicon, silicon carbide, and diamond, *J. Appl. Phys*., **35**, 3460 – 3466, (1964).

36 Cho, T.Y., Kim, Y.W.: Effect of grain growth on the thermal conductivity of liquid-phase sintered silicon carbide ceramics, *J. Eur. Ceram. Soc*., **37**, 3475 – 3481, (2017).

37 Sakai, T., Aikawa, T.: Phase transformation and thermal conductivity of hot-pressed silicon carbide containing alumina and carbon, *J. Am. Ceram. Soc*., **71**, C-7-C-9, (1988).

38 Foster, L.M., Long, G., Hunter, M.S., Reactions between aluminum oxide and carbon the Al_2O_3-Al_4C_3 phase diagram, *J. Am. Ceram. Soc*., **39**, 1 – 11, (1956).

39 Zhao, J., Lin, W., Yamaguchi, A.: Influence of heating temperature, keeping time and raw materials grain size on Al_4O_4C synthesis in carbothermal reduction process and oxidation of Al_4O_4C, *J. Ceram. Soc. Jpn*., **115**, 654 – 660, (2007).